

Hot-electron mediated ion diffusion in proton-irradiated magnesium oxide

Cheng-Wei Lee¹ and André Schleife^{1,2,3,*}

¹*Department of Materials Science and Engineering,
University of Illinois at Urbana-Champaign, Urbana, IL 61801, USA*

²*Frederick Seitz Materials Research Laboratory, University of Illinois at Urbana-Champaign, Urbana, IL 61801, USA*

³*National Center for Supercomputing Applications,
University of Illinois at Urbana-Champaign, Urbana, IL 61801, USA*

(Dated: May 18, 2022)

Highly energetic ions that impact materials have applications from semiconductor industry to medicine, and are fundamentally interesting because they trigger multi-length and time-scale processes in the target. In particular, they excite electrons into non-thermalized energy distributions, leading to subsequent non-equilibrium electron-electron and electron-ion dynamics. In order to achieve a quantitative description of these, we propose a general first-principles simulation framework that bridges time scales from ultrafast electron dynamics directly after impact, to ion diffusion over migration barriers in semiconductors. We apply it to magnesium oxide under proton irradiation and discover a diffusion mechanism that is mediated by hot electrons. Our quantitative simulations show that this mechanism strongly depends on the projectile-ion velocity, indicating that it may occur only at a specific penetration depth in the target. In addition, we predict that varying the kinetic energy of the particle radiation should open the possibility of turning this mechanism on or off, which should facilitate direct experimental observation of this effect and significantly advances current understanding of non-equilibrium electron-ion dynamics.

Energetic charged-particle radiation has exciting applications including modern research, semiconductor industry, and medicine: Helium-ion microscopy shows excellent resolution [1] and is superior to traditional electron microscopy, e.g. for insulating systems such as bio-materials [2]. Focused-ion-beam techniques achieve micro- and nano-scale structuring for photonic, plasmonic, and microelectromechanical systems [3–5]. Charged-ion therapy is becoming a competitive alternative to X-ray treatment due to better spatial control of energy deposition in the human body and, thus, reduced side effects [6, 7]. The success of all these techniques relies on a detailed, quantitative understanding of fundamental interactions between particle radiation and target material.

Highly energetic ions, carrying keV or MeV of kinetic energy, trigger multi-length- and time-scale processes in materials, depending on mass, charge, and kinetic energy of the projectile ion, the impact parameter of the scattering event, as well as the target material [8, 9]. Generally, the underlying scattering physics divides the interaction between charged-particle radiation and target into two regimes: Fast, charged particles scatter inelastically with the electronic system of the target, typically at early stages of the interaction, since the ionic system is too slow to respond. In this electronic-stopping regime, kinetic energy of particle radiation translates to electronic excitations, resulting in hot carriers. This effect manifests itself as electronic friction that slows down the projectile, rendering elastic scattering with lattice ions of the target more likely, and eventually dominating. The interaction mechanism then becomes similar to that for non-ionizing particle radiation, which has been well studied in experiment, theory, and computation [9–11].

Since high-energy projectiles significantly drive the electronic system of the target out of equilibrium, they are an ideal *probe* of otherwise hard to access, ultrafast non-equilibrium electron-ion physics [12]. Immediately after impact, the electronic system of the target is in a highly excited, *non-thermalized* state. Subsequent thermalization towards a Fermi distribution with a well-defined temperature takes tens to hundreds of femtoseconds [13–17], depending on the mechanism (e.g. electron-electron and electron-phonon scattering) and the material (semiconductors vs. metals). After thermalization, hot electrons cool over tens of picoseconds by equilibration with the lattice [18–21]. However, it is currently not well understood whether non-thermalized excited carriers, as well as thermalized hot carriers, affect atomic *diffusion*, since ion dynamics occurs on a comparable time scale of hundreds of femtoseconds, as quantified e.g. by attempt frequencies on the order of 13 THz [22].

Hence, ultrafast interactions between hot carriers and lattice ions are subject of intensive ongoing research. While ionizing radiation is known to enhance diffusion of point defects in non-metals, especially in the regime of large electronic stopping [23–25], the underlying mechanisms are not well explored. It is proposed that a change of the charge state of the defect [26, 27] significantly influences diffusion and first-principles calculations support this picture [28, 29]. However, it remains an open question how to obtain the charge state for a specific projectile and kinetic energy. Furthermore, obtaining a quantitative understanding of how hot, thermalized and non-thermalized electrons affect atomic diffusion requires an extension of the charged-defect picture.

In order to explore the impact of hot electrons on diffusivity of point defects, we devise a first-principles frame-

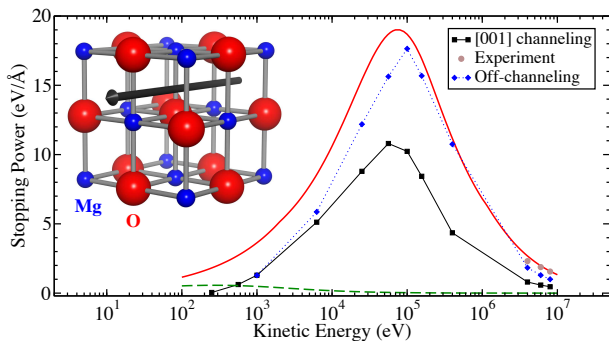


FIG. 1. (Color online.) Electronic stopping of protons in bulk rocksalt MgO. RT-TDDFT results are shown for off-channeling (blue diamonds) and [001] channel (black squares), that is indicated as black arrow in the inset. SRIM [30] simulations for a density of 3.60 g/cm^3 are shown for electronic (red solid) and nuclear (green dashed) stopping. Brown circles at high energy represent the only experiment [31] for off-channeling protons in MgO included in SRIM.

work that describes electronic response to irradiation and models the electron-ion dynamics ensuing after the initial excitation. In this work we study oxygen vacancies in magnesium oxide (MgO, see Fig. 1) as a test case for our approach, because of the simple crystal structure and extensive previous scientific study [22, 32–35]. Since a full quantum-mechanical treatment of coupled electron-ion dynamics in solids is infeasible even using state-of-the-art supercomputers, we employ cutting-edge approximations: Nuclei are described by classical Coulomb potentials, which is justified by the high projectile kinetic energy and the large mass of the ions of the target material studied here. Initially, the projectile moves too fast through the target for ions to respond and we explicitly simulate creation of electronic excitations. To compute these time-dependent hot-electron distributions we use real-time time-dependent density functional theory (RT-TDDFT) [36] in Ehrenfest molecular dynamics (EMD) simulations [37–39]. Electrons are excited at a rate that corresponds to the energy transfer from the kinetic energy of the projectile to the electronic system, typically described as electronic stopping S ,

$$S = dE/dx. \quad (1)$$

RT-TDDFT has been demonstrated to accurately describe electronic stopping in metals [39–44], semiconductors [45–50], insulators [51, 52], nanostructures [53–56], water [57, 58], and warm dense matter [59].

Explicit simulations rely on the Qb@ll [43, 60] and VASP codes [61, 62] to perform ground-state DFT calculations for MgO without (216-atom cell, Fig. 1) and with oxygen vacancy (215-atom cell, Fig. 2) with computational parameters described in Ref. 63. Time-dependent excited electronic states (see Fig. 2) are computed using EMD for a proton moving along the center of the [001]

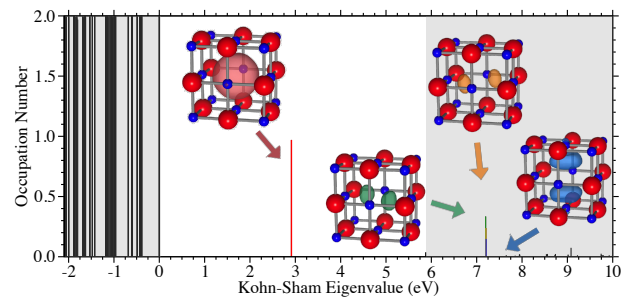


FIG. 2. (Color online.) Vertical lines indicate occupation numbers of adiabatic KS states near the band gap (unshaded area) after proton irradiation ($v=0.15 \text{ at. u.}$). Valence-band maximum is used as energy zero. Isosurfaces of partial charge density at 50 % of the maximum are shown as insets for mid-gap state (red) and first three excited localized states (green, orange, and blue, respectively).

channel closest to the oxygen vacancy, using Qb@ll [43]. Computational details are described in Ref. 64.

After the projectile traverses the simulation cell once, during which electrons are excited, it is removed and we continue EMD simulations for much longer to reveal the subsequent electron-ion dynamics. After tens of femtoseconds, depending on the velocity of the incident protons, the displacement of Mg atoms adjacent to the vacancy reaches its maximum (e.g. after 40 fs for the atom shown in inset of Fig. 4). High computational cost of these simulations, in particular for solids with point defects, prevents us from running them for long enough to explicitly study atomic diffusion for realistic migration barriers of a few eV. Instead, we explicitly compute time-dependent occupation numbers of single-particle Kohn-Sham (KS) states from EMD simulations

$$f_i(t) = \sum_{j=1} |\langle \phi_i | \psi_j(t) \rangle|^2 \quad (2)$$

where ϕ_i are the adiabatic KS ground-state orbitals of the instantaneous atomic configuration and $\psi_j(t)$ are non-adiabatic time-dependent states. We then utilize these occupations as constraint in the nudged-elastic band (NEB) method [65, 66] to compute migration barrier and defect diffusivity in the presence of hot carriers.

Figure 1 shows that our RT-TDDFT results for electronic stopping in ideal bulk MgO agree overall well with the commonly used “The Stopping and Range of Ions in Matter” (SRIM) [30] Monte Carlo package, parametrized using experimental input. While for channeling protons we observe an underestimation of electronic stopping across the entire kinetic-energy range, using an off-channeling trajectory gives rise to much better agreement between RT-TDDFT and SRIM near and past the electronic-stopping maximum. We attribute this to the reduced ability of channeling projectiles to excite semi-core electrons concentrated mostly near atomic positions

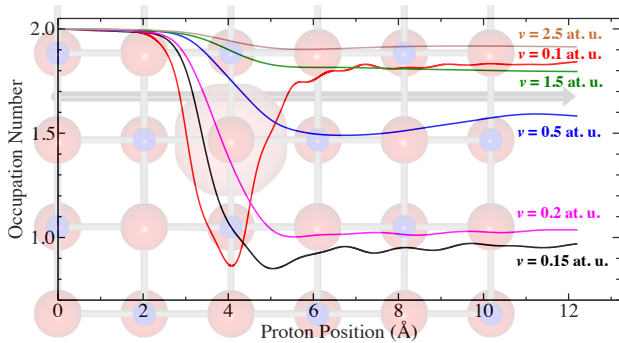


FIG. 3. (Color online.) Time evolution of the occupation number of the oxygen-vacancy mid-gap defect state during proton irradiation. The black arrow indicates the projectile trajectory. Red isosurfaces indicate partial charge density of the mid-gap state at 50 % of the maximum value.

[39, 49]. However, Fig. 1 also shows a remaining deviation at low proton kinetic energies. This can be explained by the approximate character of SRIM, which simply averages stopping of Mg and O atoms to obtain stopping for compound MgO. Since the electronic structures of Mg and O are very different and band-structure effects on electronic stopping are especially important at low kinetic energy [44, 47], the deviation is not surprising.

We further analyze how a neutral oxygen vacancy affects electronic stopping and identified two competing mechanisms, depending on the projectile kinetic energy. For slow projectiles, transitions between localized vacancy states (see Fig. 2) increase electronic stopping; the enhancement peaks for a proton velocity of $v=0.15$ at. u. (≈ 0.56 keV). Contrary, fast projectiles predominantly interact with the local charge density [46, 67] that is decreased near the vacancy, compared to a perfect crystal. This effect is more important the higher the projectile velocity, and for more than $v=1.0$ at. u., a net reduction of electronic stopping is observed, compared to ideal bulk MgO (see supplemental material at [URL will be inserted by publisher] for velocity-dependent local stopping with and without vacancy).

After studying creation of electronic excitations via electronic stopping, we now analyze those in detail using time-dependent occupation numbers, Eq. (2). In Fig. 2, we visualize these right after the proton with $v=0.15$ at. u. passed through the simulation cell once and is back close to its starting point near the cell boundary. This figure shows that the aforementioned maximum *increase* of electronic stopping due to the presence of a vacancy is attributed to excitations of almost one (0.97) electron from the vacancy-related mid-gap level, while valence states remain largely unaffected. Figure 2 also shows that the majority of this excitation, about 0.72 electrons, occupies localized, vacancy-related conduction states, labeled by arrows in Fig. 2. The remaining weight corresponds to excitations into higher-energy conduction-band states.

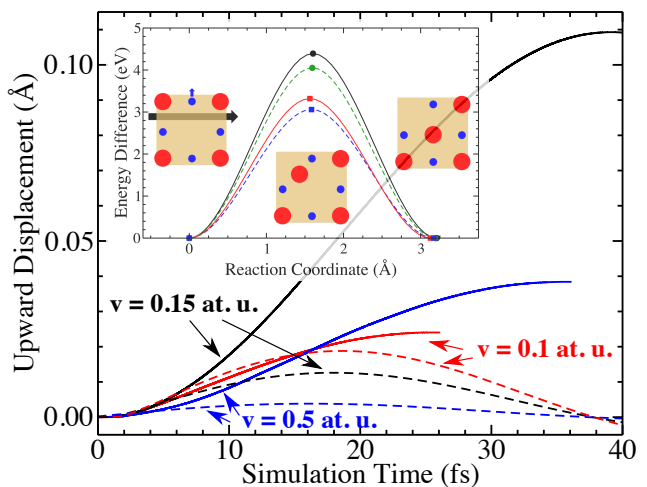


FIG. 4. (Color online.) Displacement of a Mg atom (indicated by blue arrow in inset) for projectile velocities of 0.1 at. u. (red), 0.15 at. u. (black), and 0.5 at. u. (blue). Solid and dashed lines are for EMD and Born-Oppenheimer simulations, respectively. Inset shows a diffusion path and its migration barrier computed using ground-state DFT (black circle and solid line), effective charge state (red square and solid line), Mermin DFT (green circle and dashed line), and c-DFT (blue square and dashed line) to approximate the excited state resulting from proton irradiation ($v=0.15$ at. u.).

Next, we focus on ultrafast electron dynamics and the evolution of the vacancy charge state that follows proton irradiation. To this end, we illustrate in Fig. 3 that the time-dependent number of electrons excited out of the mid-gap defect level, that shows the largest change of occupation, is strongly dependent on the proton velocity [68]. It can be seen that the largest number of electrons is excited for $v=0.15$ at. u. This coincides with the velocity for which electronic stopping is enhanced most compared to ideal bulk and, hence, directly ties the maximum stopping enhancement discussed above to a maximum depopulation of the vacancy-related mid-gap level.

In the following, we show that this localized excitation of electrons from the vacancy level due to proton irradiation significantly impacts ion dynamics. To this end, Fig. 4 compares for one Mg atom (indicated by blue arrow in the inset) the displacement that results from EMD and Born-Oppenheimer MD simulations. While Fig. 4 only shows the upward displacement of one specific Mg nearest neighbor of the initially neutral oxygen vacancy, in the supplemental material at [URL will be inserted by publisher] we provide a similar analysis for the mean-squared displacement of all first and second nearest neighbors, leading to similar conclusions.

Our analysis clearly indicates that, depending on the projectile kinetic energy, the displacement is enhanced by up to one order of magnitude in the presence of electronic excitations, compared to Born-Oppenheimer dynamics in the electronic ground state. Figure 4 also shows that the

vibrational period increases by about a factor of up to 2.2 in the presence of excited electrons. Finally, this figure illustrates that EMD simulations predict the largest displacement of the nearest-neighbor Mg atom for proton irradiation with $v=0.15$ at. u. This is consistent with our earlier discussion that the maximum depopulation of the vacancy-defect level (see Fig. 3) and the maximum enhancement of electronic stopping occur for that same velocity and, hence, are related to that state. We note that this maximum Mg displacement corresponds to an effective maximum opening of the diffusion path for oxygen shown in the inset of Fig. 4, induced by radiation of a certain kinetic energy ($v=0.15$ at. u.). Born-Oppenheimer MD qualitatively differs by finding much smaller maximum displacement that occurs for the lowest projectile velocity (see Fig. 4), since this corresponds to the longest interaction time of the proton with the Mg atom. This clearly highlights the intimate coupling of electronic excitations and ionic motion.

To understand this further, we note that the vacancy-related mid-gap level is localized, as can be seen in the insets of Fig. 2, and occupied with two bonding electrons in its ground state [33]. The excitation of electrons from this state into higher-energy vacancy-related states, the corresponding displacement of nearest-neighbor Mg atoms, and the increased oscillation period discussed above can be understood within the bond-softening model [69]: The removal of electrons from the bonding state due to proton irradiation causes bond weakening, or softening, and, thus, a displacement of atoms near the vacancy away from it. Our EMD simulations quantitatively predict the underlying electron dynamics as well as the resulting motion of ions. While longer EMD simulations would be desirable to understand these processes better, they are prohibitively expensive even on state-of-the-art supercomputers.

Instead, to quantify hot-electron mediated ion diffusion, we analyze the jump frequency Γ in an Arrhenius equation for tracer diffusion using transition-state theory [70],

$$\Gamma = \nu^* \exp(-\Delta E_m/k_B T), \quad (3)$$

with ν^* as attempt frequency and ΔE_m as migration barrier. The diffusivity D is proportional to Γ and all prefactors are assumed to be constant. In particular, we consider dynamics at short time scales, which justifies the assumption that there is a constant equilibrium concentration of oxygen vacancies. Hence, in the following we quantify the influence of hot electrons on diffusivity via ν^* and ΔE_m .

Computing the Einstein frequency via finite-difference displacements of 0.01 Å allows us to calculate ν^* using the Vineyard expression [71]. From this we find results comparable to 13 THz reported in the literature for oxygen atoms in MgO [22] (see supplemental material at [URL will be inserted by publisher] for explicit results for

ν^*). We evaluate ΔE_m by combining constrained DFT (c-DFT) and the climbing-image NEB method [65, 66] as implemented based on the VASP code.

Most importantly, when computing ν^* and ΔE_m , we apply an occupation-number constraint within c-DFT to account for the hot-electron distribution after proton irradiation in finite-difference as well as NEB calculations. Here we compare three different approximations for this constraint: (i) KS occupation numbers computed from EMD using Eq. (2) represent the most accurate reference immediately after the excitation. (ii) Alternatively, we use an approach that does not explicitly describe electronic excitations, by assuming that only the charge state of the vacancy is changed as a consequence of proton irradiation. This is motivated by previous studies [28, 29], and our observation that at most one electron is excited out of the vacancy-related mid-gap level (see Fig. 3). We use the occupation number of the mid-gap state from our EMD simulation, which is 0.97, as reported above. (iii) For additional comparison, we model hot, fully *thermalized* electrons within Mermin DFT using KS occupation numbers that correspond to an effective Fermi temperature [72–74]. To this end, we compute the total-energy change upon excitation of the defect level by the proton (see supplemental material at [URL will be inserted by publisher] for detailed description of this procedure). Neglecting entropy differences, we estimate the Fermi temperature as the temperature that leads to the same total-energy difference and find $T=9211$ K for $v=0.15$ at. u.

From this analysis we find that all three occupation constraints, that we use to mimic hot-electron distributions, give rise to enhanced atomic diffusion compared to the ground-state case and, in particular, result in lower migration barriers ΔE_m (see inset of Fig. 4). The values of ΔE_m are 0.34 eV, 1.07 eV, and 1.33 eV lower than the ground-state barrier of ≈ 4.4 eV when Mermin DFT, fixed-charge model, and c-DFT are used, respectively. The difference between c-DFT and Mermin DFT is related to the underlying time scale: c-DFT is the better approximation at early stages after proton irradiation, i.e., well before thermalized, excited electrons dominate over non-thermalized ones. While this is a heavily debated question, early tests (see supplemental material at [URL will be inserted by publisher] for discussion of the long-term evolution of occupation numbers) indicate that this is the case for the first several tens of femtoseconds after irradiation, during which Mermin DFT is not adequate. The fixed-charge model predicts results closer to those of c-DFT, highlighting that both the charge state of the point defect as well as the excited-electron distribution enhance atomic diffusion.

The influence of hot-electron distributions on the phonon frequency and, thus, the attempt frequency ν^* is more complicated: We find slightly enhanced (+1.10%), significantly enhanced (+19.85%), and reduced (−6.61%) attempt frequencies within the fixed-

charge model, Mermin DFT, and c-DFT, respectively. However, while excited-electron distributions affect both the migration barrier as well as the attempt frequency, overall the migration barrier dominates the resulting diffusivity. This is because the change of ΔE_m due to hot electrons discussed above is significant and Eq. (3) unveils an exponential dependence of Γ on ΔE_m . The 20 % change of the effective jump rate discussed above is much smaller compared to the change in diffusivity, e.g. for a specific example of $T=900$ K. In this case, the difference in diffusivity between the migration barrier calculated using ground-state DFT (≈ 4.4 eV) and c-DFT (≈ 3.1 eV) is on the order of 10^7 . This shows that there is a tremendous hot-electron induced increase of diffusivity during the early stages of radiation damage.

In summary, we devise a fully first-principles simulation framework to quantitatively study hot-electron mediated ion diffusion, by combining real-time time-dependent density functional theory, occupation-number constraints, and the nudged-elastic band method. Our parameter-free technique bridges time scales ranging from ultrafast, electronic-excitation dynamics all the way to ion diffusion across migration barriers of several eV. We apply this framework to magnesium oxide with and without an oxygen vacancy, as an important test bed material. Using our results, we discover a novel diffusion mechanism that derives from a significant lowering of migration energies in the presence of non-thermalized as well as thermalized carriers. We observe a strong dependence of this mechanism on the kinetic energy of the projectile and attribute this to excitations of specific defect electrons. This implies that hot-electron mediated ion diffusion is defect-specific and, for each defect, occurs only at a specific penetration depth of the projectile in the target, where it can efficiently excite defect electrons. Furthermore, our findings illustrate a possible route towards deliberate diffusion enhancement by irradiating with projectiles of a specific kinetic energy. We envision that this can be used to actively enhance or suppress defect diffusion by tuning the energy of the ion beam.

Fruitful discussions with Ravi Agarwal, Xavier Andrade, Alfredo Correa, Yosuke Kanai, and Pascal Pochet are gratefully acknowledged. Financial support from the Sandia National Laboratory-UIUC collaboration is acknowledged (SNL grant no. 1736375). C.-W. L. acknowledges support from the Government Scholarship to Study Abroad from the Taiwan Ministry of Education. An award of computer time was provided by the Innovative and Novel Computational Impact on Theory and Experiment (INCITE) program. This research used resources of the Argonne Leadership Computing Facility, which is a DOE Office of Science User Facility supported under Contract DE-AC02-06CH11357. Data used in this work are available at the Materials Data Facility [75, 76].

-
- * schleife@illinois.edu
- [1] B. W. Ward, J. A. Notte, and N. P. Economou, *J. Vac. Sci. Technol. B* **24**, 2871 (2006).
 - [2] M. S. Joens, C. Huynh, J. M. Kasuboski, D. Ferranti, Y. J. Sigal, F. Zeitvogel, M. Obst, C. J. Burkhardt, K. P. Curran, S. H. Chalasani, L. A. Stern, B. Goetze, and J. A. J. Fitzpatrick, *Sci. Rep.-UK* **3**, 3514 EP (2013).
 - [3] C.-S. Kim, S.-H. Ahn, and D.-Y. Jang, *Vacuum* **86**, 1014 (2012).
 - [4] N. C. Lindquist, P. Nagpal, K. M. McPeak, D. J. Norris, and S.-H. Oh, *Rep. Prog. Phys.* **75**, 036501 (2012).
 - [5] A. V. Krashennnikov and K. Nordlund, *J. Appl. Phys.* **107**, 071301 (2010).
 - [6] M. Durante and J. S. Loeffler, *Nat. Rev. Clin. Oncol.* **7**, 37 (2010).
 - [7] D. Scharadt, T. Elsässer, and D. Schulz-Ertner, *Rev. Mod. Phys.* **82**, 383 (2010).
 - [8] A. A. Correa, *Comput. Mater. Sci.* **150**, 291 (2018).
 - [9] B. Wirth, G. Odette, J. Marian, L. Ventelon, J. Young-Vandersall, and L. Zepeda-Ruiz, *J. Nucl. Mater.* **329-333**, 103 (2004), proceedings of the 11th International Conference on Fusion Reactor Materials (ICFRM-11).
 - [10] R. S. Averback and T. D. de la Rubia, *Solid State Phys.* **51**, 281 (1997).
 - [11] M. Raine, A. Jay, N. Richard, V. Goiffon, S. Girard, M. Gaillardin, and P. Paillet, *IEEE T. Nucl. Sci.* **64**, 133 (2017).
 - [12] T. Susi, J. Kotakoski, D. Kepaptsoglou, C. Mangler, T. C. Lovejoy, O. L. Krivanek, R. Zan, U. Bangert, P. Ayala, J. C. Meyer, and Q. Ramasse, *Phys. Rev. Lett.* **113**, 115501 (2014).
 - [13] Z. Nie, R. Long, L. Sun, C.-C. Huang, J. Zhang, Q. Xiong, D. W. Hewak, Z. Shen, O. V. Prezhdo, and Z.-H. Loh, *ACS Nano* **8**, 10931 (2014).
 - [14] M. Bernardi, D. Vigil-Fowler, J. Lischner, J. B. Neaton, and S. G. Louie, *Phys. Rev. Lett.* **112**, 257402 (2014).
 - [15] V. A. Jhalani, J.-J. Zhou, and M. Bernardi, *Nano Lett.* **17**, 5012 (2017).
 - [16] J. M. Richter, F. Branchi, F. Valduga de Almeida Camargo, B. Zhao, R. H. Friend, G. Cerullo, and F. Deschler, *Nat. Commun.* **8**, 376 (2017).
 - [17] H. Harutyunyan, A. B. F. Martinson, D. Rosenmann, L. K. Khorashad, L. V. Besteiro, A. O. Govorov, and G. P. Wiederrecht, *Nat. Nanotechnol.* **10**, 770 (2015).
 - [18] T. G. White, P. Mabey, D. O. Gericke, N. J. Hartley, H. W. Doyle, D. McGonegle, D. S. Rackstraw, A. Higginbotham, and G. Gregori, *Phys. Rev. B* **90**, 014305 (2014).
 - [19] M.-F. Lin, V. Kochat, A. Krishnamoorthy, L. Bassman, C. Weninger, Q. Zheng, X. Zhang, A. Apte, C. S. Tiwary, X. Shen, R. Li, R. Kalia, P. Ajayan, A. Nakano, P. Vashishta, F. Shimozono, X. Wang, D. M. Fritz, and U. Bergmann, *Nat. Commun.* **8**, 1745 (2017).
 - [20] H. E. Elsayed-Ali and T. Juhasz, *Phys. Rev. B* **47**, 13599 (1993).
 - [21] S. Sadasivam, M. K. Y. Chan, and P. Darancet, *Phys. Rev. Lett.* **119**, 136602 (2017).
 - [22] O. Runevall and N. Sandberg, *J. Phys-Condens. Mat.* **23**, 345402 (2011).
 - [23] S. Zinkle, *J. Nucl. Mater.* **219**, 113 (1995).
 - [24] S. Zinkle and L. Snead, *Scripta Mater.* **143**, 154 (2018).

- [25] Y. Zhang, R. Sachan, O. H. Pakarinen, M. F. Chisholm, P. Liu, H. Xue, and W. J. Weber, *Nat. Commun.* **6**, 8049 (2015).
- [26] S. J. Zinkle, *MRS Proceedings* **439**, 667 (1996).
- [27] J. C. Bourgoin, *Radiat. Eff. Defect. S.* **111-112**, 29 (1989).
- [28] Y. Lei and G. Wang, *Scripta Mater.* **101**, 20 (2015).
- [29] J. Mulroue and D. M. Duffy, *P. Roy. Soc. Lond. A Mat.* **467**, 2054 (2011).
- [30] J. F. Ziegler, M. D. Ziegler, and J. P. Biersack, *Nucl. Instrum. Meth. B* **268**, 1818 (2010).
- [31] G. J. Clark, D. V. J. C. Morgan, and J. M. Poate, in *Atomic collision phenomena in solids*, edited by D. Palmer, M. Thompson, and Townsend (North-Holland Pub. Co., 1970) Chap. 10, pp. 388–399.
- [32] D. Alfè and M. J. Gillan, *Phys. Rev. B* **71**, 220101 (2005).
- [33] P. Rinke, A. Schleife, E. Kioupakis, A. Janotti, C. Rödl, F. Bechstedt, M. Scheffler, and C. G. Van de Walle, *Phys. Rev. Lett.* **108**, 126404 (2012).
- [34] E. Ertekin, L. K. Wagner, and J. C. Grossman, *Phys. Rev. B* **87**, 155210 (2013).
- [35] S. kang Lin, C. kuei Yeh, B. Puchala, Y.-L. Lee, and D. Morgan, *Comput. Mater. Sci.* **73**, 41 (2013).
- [36] E. Runge and E. K. U. Gross, *Phys. Rev. Lett.* **52**, 997 (1984).
- [37] P. Ehrenfest, *Z. Phys. A* **45**, 455 (1927).
- [38] D. Marx and H. Jurg, *Ab Initio Molecular Dynamics: Basic Theory and Advanced Methods* (Cambridge University Press, 2009).
- [39] A. Schleife, Y. Kanai, and A. A. Correa, *Phys. Rev. B* **91**, 014306 (2015).
- [40] A. A. Correa, J. Kohanoff, E. Artacho, D. Sánchez-Portal, and A. Caro, *Phys. Rev. Lett.* **108**, 213201 (2012).
- [41] M. A. Zeb, J. Kohanoff, D. Sánchez-Portal, A. Arnau, J. I. Juaristi, and E. Artacho, *Phys. Rev. Lett.* **108**, 225504 (2012).
- [42] G. Bi, J. Kang, and L.-W. Wang, *Phys. Chem. Chem. Phys.* **19**, 9053 (2017).
- [43] A. Schleife, E. W. Draeger, V. M. Anisimov, A. A. Correa, and Y. Kanai, *Comput. Sci. Eng.* **16**, 54 (2014).
- [44] E. E. Quashie, B. C. Saha, and A. A. Correa, *Phys. Rev. B* **94**, 155403 (2016).
- [45] R. Hatcher, M. Beck, A. Tackett, and S. T. Pantelides, *Phys. Rev. Lett.* **100**, 103201 (2008).
- [46] R. Ullah, F. Corsetti, D. Sánchez-Portal, and E. Artacho, *Phys. Rev. B* **91**, 125203 (2015).
- [47] A. Lim, W. M. C. Foulkes, A. P. Horsfield, D. R. Mason, A. Schleife, E. W. Draeger, and A. A. Correa, *Phys. Rev. Lett.* **116**, 043201 (2016).
- [48] D. C. Yost and Y. Kanai, *Phys. Rev. B* **94**, 115107 (2016).
- [49] D. C. Yost, Y. Yao, and Y. Kanai, *Phys. Rev. B* **96**, 115134 (2017).
- [50] C.-W. Lee and A. Schleife, (2018), arXiv:1803.10182.
- [51] J. M. Pruneda, D. Sánchez-Portal, A. Arnau, J. I. Juaristi, and E. Artacho, *Phys. Rev. Lett.* **99**, 235501 (2007).
- [52] C.-K. Li, F. Wang, B. Liao, X.-P. OuYang, and F.-S. Zhang, *Phys. Rev. B* **96**, 094301 (2017).
- [53] A. V. Krashennnikov, Y. Miyamoto, and D. Tománek, *Phys. Rev. Lett.* **99**, 016104 (2007).
- [54] M. Quijada, A. G. Borisov, I. Nagy, R. Díez Muiño, and P. M. Echenique, *Phys. Rev. A* **75**, 042902 (2007).
- [55] A. Ojanperä, A. V. Krashennnikov, and M. Puska, *Phys. Rev. B* **89**, 035120 (2014).
- [56] Z. Wang, S.-S. Li, and L.-W. Wang, *Phys. Rev. Lett.* **114**, 063004 (2015).
- [57] K. G. Reeves, Y. Yao, and Y. Kanai, *Phys. Rev. B* **94**, 041108 (2016).
- [58] K. G. Reeves and Y. Kanai, *Sci. Rep.-UK* **7**, 40379 (2017).
- [59] R. J. Magyar, L. Shulenburger, and A. D. Baczewski, *Contrib. Plasm. Phys.* **56**, 459 (2016).
- [60] E. W. Draeger and F. Gygi, “Qbox code, qb@ll version,” (2017), Lawrence Livermore National Laboratory.
- [61] G. Kresse and D. Joubert, *Phys. Rev. B* **59**, 1758 (1999).
- [62] G. Kresse and J. Furthmüller, *Phys. Rev. B* **54**, 11169 (1996).
- [63] Kohn-Sham states are expanded into a plane-wave basis and the local-density approximation is used to describe exchange and correlation [77, 78]. The electron-ion interaction is described either by the projector-augmented wave technique [61, 62] (VASP) or norm-conserving Hamann, Schlüter, and Chiang pseudopotentials as modified by Vanderbilt [79] (Qb@ll). Plane wave cutoffs are 120 Ry (Qb@ll) and 600 eV (VASP) to obtain converged results using the criteria of 5 meV/atom. The Γ point is used to sample the Brillouin zone, which is justified for the large simulations cells used here. After starting from a relaxed lattice constant of 4.070 Å (Qb@ll) and 4.165 (VASP) Å, atomic positions are fully relaxed until the forces are less than 5 meV/Å.
- [64] Time-dependent KS equations are propagated in real time using a fourth-order Runge-Kutta integrator [80]. Hellman-Feynman forces are computed from the time-dependent electron density [37, 38]. For comparison we also perform Born-Oppenheimer [81] molecular dynamics simulations using Qb@ll.
- [65] G. Henkelman and H. Jónsson, *J. Chem. Phys.* **113**, 9978 (2000).
- [66] G. Henkelman, B. P. Uberuaga, and H. Jónsson, *J. Chem. Phys.* **113**, 9901 (2000).
- [67] H. Winter, J. I. Juaristi, I. Nagy, A. Arnau, and P. M. Echenique, *Phys. Rev. B* **67**, 245401 (2003).
- [68] For convenience, the atomic configuration at $t=0$ was used as reference state for Fig. 3. However, we emphasize that the difference compared to using the atomic configuration at time t is insignificant, since the atomic movement is very small on this time scale.
- [69] N. Itoh, D. M. Duffy, S. Khakshouri, and A. M. Stoneham, *J. Phys.-Condens. Mat.* **21**, 474205 (2009).
- [70] H. Eyring, *J. Chem. Phys.* **3**, 107 (1935).
- [71] G. H. Vineyard, *J. Phys. Chem. Solids* **3**, 121 (1957).
- [72] N. D. Mermin, *Phys. Rev.* **137**, A1441 (1965).
- [73] A. Alavi, J. Kohanoff, M. Parrinello, and D. Frenkel, *Phys. Rev. Lett.* **73**, 2599 (1994).
- [74] P. L. Silvestrelli, A. Alavi, M. Parrinello, and D. Frenkel, *Phys. Rev. Lett.* **77**, 3149 (1996).
- [75] B. Blaiszik, K. Chard, J. Pruyne, R. Ananthakrishnan, S. Tuecke, and I. Foster, *JOM* **68**, 2045 (2016).
- [76] C.-W. Lee and A. Schleife, (2018), 10.18126/M2C35K.
- [77] D. M. Ceperley and B. J. Alder, *Phys. Rev. Lett.* **45**, 566 (1980).
- [78] J. P. Perdew and A. Zunger, *Phys. Rev. B* **23**, 5048 (1981).
- [79] D. Vanderbilt, *Phys. Rev. B* **32**, 8412 (1985).
- [80] A. Schleife, E. W. Draeger, Y. Kanai, and A. A. Correa, *J. Chem. Phys.* **137**, 22A546 (2012).
- [81] M. Born and R. Oppenheimer, *Ann. Phys.-Berlin* **389**,

457 (1927).